Screening the Cytotoxicity of Single-Walled Carbon Nanotubes Using Novel 3D Tissue-Mimetic Models

Dania Movia,[†,‡] Adriele Prina-Mello,[†,§] Despina Bazou,[†,⊥] Yuri Volkov,[†,§,*] and Silvia Giordani[†,‡,*]

[†]Centre for Research on Adaptive Nanostructures and Nanodevices (CRANN), [‡]School of Chemistry, [§]School of Medicine, and [⊥]School of Pharmacy and Pharmaceutical Sciences, Trinity College Dublin, Ireland

ABSTRACT

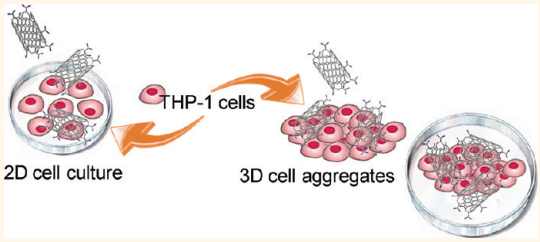

Single-walled carbon nanotubes (SWNTs) are promising candidates for a wide range of biomedical applications due to their fascinating properties. However, safety concerns are raised on their potential human toxicity and on the techniques that need to be used to assess such toxicity. Here, we integrate for the first time 3D tissue-mimetic models in the cytotoxicity assessment of purified (p-) and oxidized (o-) SWNTs. An established ultrasound standing wave trap was used to generate the 3D cell aggregates, and results were compared with traditional 2D cell culture models. Protein-based (bovine serum albumin) and surfactant-based (Pluronic F68) nanotube dispersions were tested and compared to a reference suspension in dimethyl sulfoxide. Our results indicated that p- and o-SWNTs were not toxic in the 3D cellular model following a 24 h exposure. In contrast, 2D cell cultures were significantly affected by exposure to p- and o-SWNTs after 24 h, as assessed by high-content screening and analysis (HCSA). Finally, cytokine (IL-6 and TNF-α) secretion levels were elevated in the 2D but remained essentially unchanged in the 3D cell models. Our results strongly indicate that 3D cell aggregates can be used as alternative *in vitro* models providing guidance on nanomaterial toxicity in a tissue-mimetic manner, thus offering future cost-effective solutions for toxicity screening assays under the experimental conditions more closely related to the physiological scenario in 3D tissue microenvironments.

KEYWORDS: single-walled carbon nanotubes · macrophages · high-content screening and analysis · 3D tissue-mimetic cell cultures · toxicity · ultrasound standing wave trap

Synthetic carbon allotropes, such as single-walled carbon nanotubes (SWNTs), represent a growing family of fascinating nanomaterials with outstanding properties that are relevant in many potential applications, ranging from synthetic materials to drug delivery systems.[1] SWNTs' unique properties (such as size, shape, and composition), however, raise concerns about their potential human toxicity,[2,3] while their diversity from bulk materials poses significant challenges over traditional toxicity-screening approaches.[4]

The test system currently employed for assessing the toxicity of chemical substances was introduced over 80 years ago.[4] Only a few changes have been incorporated over the past decades, thus leaving the screening procedures almost unchanged and the experimental protocols obsolete when testing nanomaterials.[4,5] A three-step scheme has been recently proposed as a solution by Hartung,[4] and it is described as follows: (1) define the limitations of current tools; (2) combine them in a strategic way; and finally (3) develop a new testing system that integrates the old set of testing protocols with modern technologies. Among the latest, Hartung proposed imaging techniques and robotized testing platforms (such as high-content screening and analysis (HCSA)), *in silico* methods (heatmaps and quantitative structure−activity relationship (QSAR)), advanced cell-culturing techniques (three-dimensional "organotypic" cell cultures), and "omics" technologies (genomics and proteomics).[4] While HCSA[6−12] and *in silico* methods[8,13] are commonly recognized and exploited as important techniques for the assessment of nanomaterials toxicity, the use of three-dimensional (3D) *in vitro* cell models (that can better represent the 3D organization of tissues *in vivo* compared to the conventional 2D cell cultures[14,15]) is still at its infancy within the nanotoxicology field. 3D cell aggregates more closely resemble the *in vivo* situation with regard to cell shape and cellular environment,[16] which can in turn regulate the gene expression and hence the biological behavior of cells.[17] To the best of our knowledge, only a few studies used coculture systems[18,19] and/or 3D cell cultures

Received for review September 23, 2011 and accepted October 21, 2011.

Published online October 21, 2011
10.1021/nn203659m

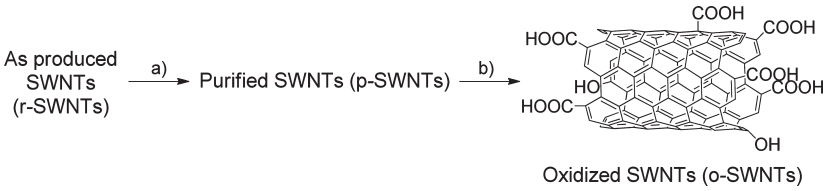

Scheme 1. Purification and oxidation of as-produced HiPCO SWNTs (r-SWNTs):[31] (a) HNO_3 2.6 M, 100 °C, 48 h; (b) $H_2SO_4 \cdot H_2O_2$ (4:1), 35 °C, 1 h.

for testing nanomaterial toxicity.[20,21] However, no "organotypic" cell culture technique has been employed to date for the assessment of SWNT toxicity.

The purpose of the present study is to assess the cytotoxicity of high-pressure carbon monoxide (HiPCO) SWNTs using 3D cellular, tissue-mimetic models. A comparative approach determining the importance of the third dimension in cell culture is presented. The THP-1 cell line, a macrophage model, was employed to represent the resident phagocytic cells (*i.e.*, monocytes and macrophages) located in the liver (Kupffer cells)[22] that have the main function of removing pathogens, senescent cells, and external particles from the bloodstream.[23] Since the liver is a preferential site of nanomaterial accumulation in humans and rats,[22,24] THP-1 cells may be exploited as a close equivalent of key indicative phagocytic cell populations responding to carbon nanotubes (CNTs). This cell line has been previously employed to gain insight into the potential effects of SWNTs in the liver.[22] We acknowledge that macrophage responses do not provide a full indication of potential toxic effects in the body; nevertheless, this cellular model offers good cytotoxicity prediction information, particularly in the early phases of investigations.[25,26]

Our results showed for the first time that the cytotoxicity of purified (p-SWNTs) and oxidized (o-SWNTs) SWNTs was not detectable in the 3D cellular model following a 24 h exposure. In contrast, 2D cell cultures were significantly affected by exposure to p- and o-SWNTs after 24 h, as assessed by viability and multifluorescence-based cell assays. In conjunction with the previously reported study on nanoparticle cytotoxicity in 3D cell cultures,[20] our data clearly underline the importance of incorporating 3D "tissue-mimetic" cell models in the assessment of SWNT toxicity and strongly advocate the pressing need for the redefinition of the established nanotoxicology protocols.

RESULTS AND DISCUSSION

Since the intrinsic toxicity of as-produced (r-SWNTs) SWNTs is reported to decrease with removal of toxic metal impurities,[27−29] and with reducing the length of the tubes,[30] r-SWNTs were purified and oxidized following a previously reported procedure[31] (Scheme 1).

Physicochemical Characterization. Complete physicochemical characterization of the tested material is required nowadays to enhance the validity of the performed toxicity studies.[5,32−36] A thorough characterization of the impurities content, lengths, and electronic properties of p- and o-SWNTs has been previously reported,[31] showing that p- and o-SWNTs are able to emit efficiently in the NIR despite the employment of strong chemical treatments that shorten the tubes and introduce defect sites on the nanotube surface.[31] In this study, NIR-photoluminescence (PL) spectroscopy (Figure 1) and zeta potential measurements (Table 1) were carried out on p- and o-SWNTs dispersed in deionized (DI) water or RPMI 1640 cell media. Taking into account that (1) the dispersion grade of CNTs in the biological media can affect both their *in vitro*[37] and *in vivo*[38] toxicity, (2) bundles of SWNTs can be disrupted *via* noncovalent functionalization with surfactants,[39,40] and (3) *in vitro* cell responses seem to depend strongly on the surfactant employed,[37,41,42] we introduced both a protein-based (bovine serum albumin, BSA) and a surfactant-based (Pluronic F68) methodology for dispersing p- and o-SWNTs in an aqueous/biological environment. BSA is a water-soluble globular protein that has been shown to adsorb on the CNT surface[43,44] and to have an excellent dispersing capability[45] even in *in vitro* conditions.[46] BSA is characterized by a pH-sensitive tertiary structure,[47,48] which strongly affects its capability of stabilizing CNT dispersions at varying pH.[49] Better-dispersed SWNT solutions are achieved at pH ranging between 4 and 8,[49] which was in agreement with our study where all SWNT solutions had a neutral pH (pH = 6−7). Pluronic F68 is a biocompatible,[50] linear copolymer of isopropylene glycol repeating units, with properties very similar to a nonionic surfactant.[51] Pluronic F68 is able to stabilize an aqueous dispersion of SWNTs,[52] and copolymers of the Pluronic family are successfully adopted in the toxicity testing of CNTs.[38,53] SWNT dispersions in DMSO were used as reference. For consistency both p- and o-SWNTs were dispersed in DMSO.

NIR-PL spectroscopy (Figure 1) was employed to clarify the stability of p- and o-SWNTs in RPMI 1640 cell media over time. NIR fluorescence is the optical property of SWNTs that is most sensitive to sample dispersion grade. Aggregation of isolated nanotubes prevents in fact the luminescence of SWNTs[54,55] and reduces PL intensity.[55−58] NIR-PL spectra showed that p- (Figure 1a) and o-SWNTs (Figure 1e) dispersed in RPMI 1640 media emitted more efficiently when the cell media was supplemented with BSA or Pluronic F68,

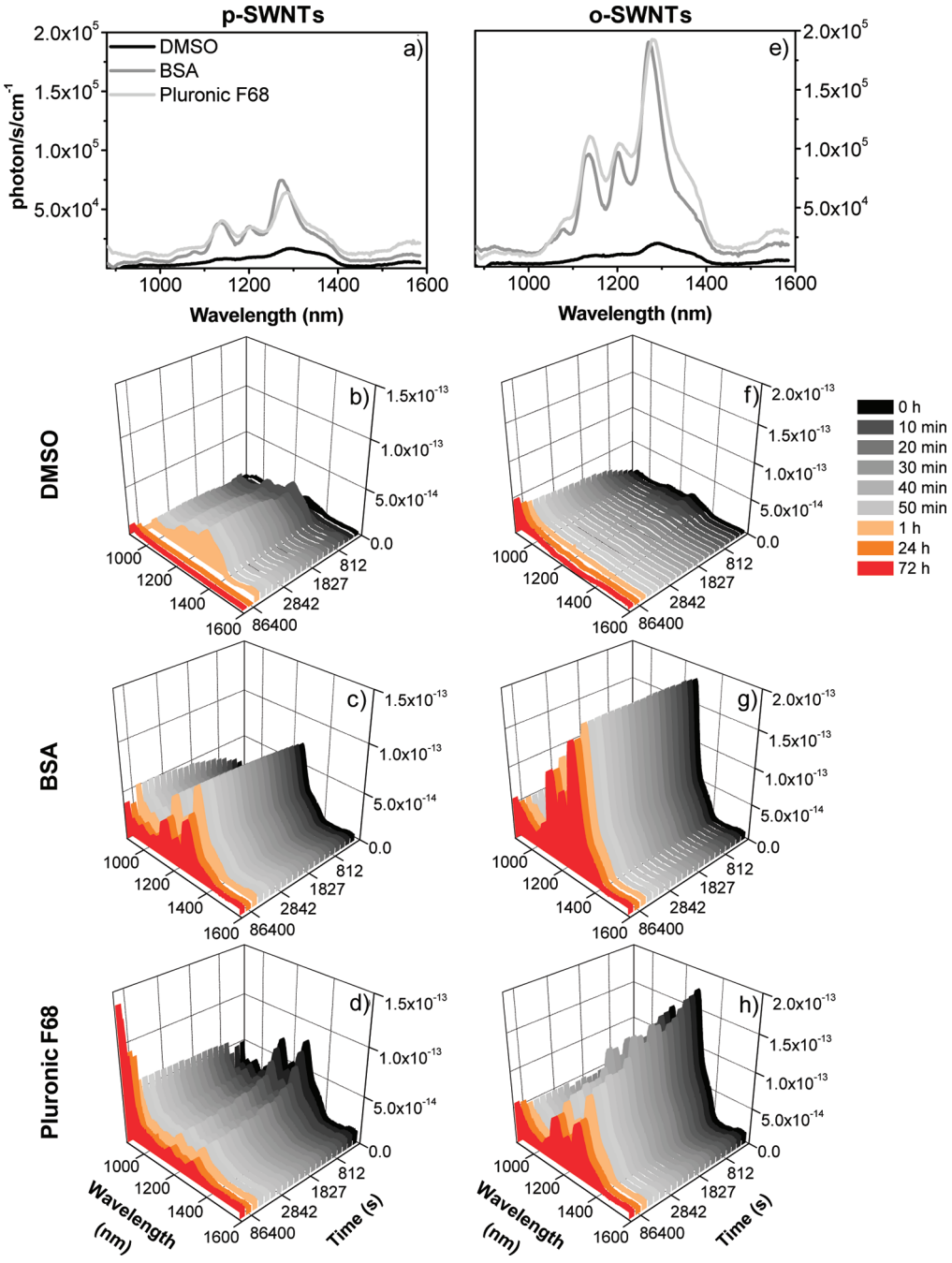

Figure 1. NIR-PL spectra (λ_{exc} = 683 nm) of (a−d) p- and (e−h) o-SWNTs dispersed in supplemented RPMI 1640 cell media ([SWNTs]$_i$ = 120 μg/mL) with or without the addition of a dispersing agent (BSA or Pluronic F68). Graphs (b−d; f−h) show the changes of NIR-PL of (b, f) DMSO-, (c, g) BSA-, and (d, h) Pluronic F68-stabilized dispersions over 1 h (black to light orange curves), after 24 h (orange curves) and after 72 h (red curves).

suggesting that better dispersions were achieved by addition of BSA and Pluronic F68. Shifts in the position of the NIR-PL peaks were shown when BSA or Pluronic F68 was added, thus confirming the interaction of such dispersing agents with the nanotubes' surface. In addition, the NIR-PL intensity of o-SWNTs (Figure 1e) was higher than that of p-SWNTs (Figure 1a). This result suggested that the more hydrophilic o-SWNTs were better dispersed in cell media than p-SWNTs. Interestingly, Pluronic F68 was less effective than BSA in stabilizing p- and o-SWNTs dispersions over time. The NIR-PL intensity of Pluronic F68-stabilized dispersions decreased significantly with time (Figure 1d, h), whereas BSA was capable of forming dispersions that were stable over 2 days (Figure 1c, g). This result found rationalization in the remarkable property of BSA to stabilize SWNT aqueous solutions even in the presence of monocationic (Na^+) and dication (Ca^{2+}) ions.[59]

Similar to previously reported findings,[59−62] zeta potential measurements evidenced a negative surface

TABLE 1. Surface Charges of p- and o-SWNTs before and after Dispersion in Supplemented RPMI 1640 Cell Media at Three Different Concentrations (120, 60, and 12 μg/mL)

		zeta potential (mV)[a]					
		DMSO[b]		BSA[b]		Pluronic F68[b]	
SWNTs	dose (μg/mL)	DI water	RPMI 1640	DI water	RPMI 1640	DI water	RPMI 1640
p-SWNTs	120	−23.6	−2.7	−30.3	−9.3	−14.1	−0.9
	60	−21.0	−6.5	−12.9	−11.1	−13.1	−10.6
	12	−27.8	−2.0	−33.4	−14.4	−17.0	−11.5
o-SWNTs	120	−40.2	−2.9	−9.2	−2.8	−29.8	−1.1
	60	−58.4	−4.7	−33.2	−1.2	−41.7	−1.9
	12	−38.2	−0.4	−41.3	−0.8	−43.3	−0.4

[a] Surface charges were measured in DI water or in RPMI 1640 cell media. [b] Dispersing agent added as described in the Experimental Section.

potential for both p- and o-SWNTs in DI water or in supplemented RPMI 1640 cell media at neutral pH (Table 1), with or without addition of dispersing agents (BSA or Pluronic F68). In DI water, o-SWNTs possessed increased absolute values of zeta potential when compared to p-SWNTs. This may be due to the negative surface charges associated with the dissociated carboxylic groups (COO^-) on their surface[63] or to the higher dispersibility of the more hydrophilic o-SWNTs in water (dispersions with zeta potential above +30 mV or below −30 mV correspond to stable solutions[64]). Yet the coexistence of the two phenomena is possible. A decrease in the absolute values of zeta potential was registered when both p- and o-SWNTs were suspended in RPMI 1640 cell media, suggesting that the dispersions stability decreased. Similar to what is observed with aqueous colloidal particles[64] and to what is reported in previous studies on carbon nanotubes,[59,60] our results are attributed to the high ionic strength of RPMI 1640 cell media that suppressed the electrostatic repulsion among tubes. Notably, p-SWNTs dispersions in RPMI 1640 cell media had higher zeta potential than o-SWNTs suspensions. As shown by NIR-PL data, this is not associated with a higher stability of p-SWNTs in RPMI 1640 media, whereas it can be explained by the passivation of the COO^- attached onto the o-SWNT surface by the positively charged components (such as cations, proteins) of the cell media.

High Content Screening and Analysis of 2D Cell Cultures. As per Hartung's guidelines,[4] we chose the HCSA system as the ideal tool for simultaneously detecting changes in many cellular properties, thus producing a comprehensive set of data that provide guidance on the toxic response of a whole organism.[65] Cell viability, cell membrane permeability, lysosomal mass/pH, and nuclear staining intensity changes are the parameters commonly used for evaluating the cellular cytotoxicity of chemical compounds,[66] drugs, and nanomaterials.[9,67,68] Three different concentrations (120, 60, and 12 μg/mL) of p- and o-SWNTs were tested on populations of 20 000 cells.

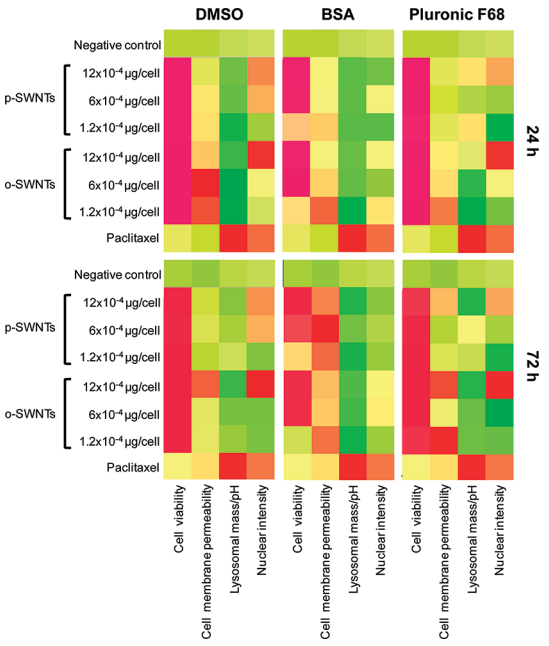

Figure 2. Graphical response intensity tables (heatmaps) of multiparametric HCSA data for 2D cell cultures exposed to p- and o-SWNTs for 24 and 72 h. Colorimetric gradient tables reflect the cytoxicity evolution by showing the cell viability (left column), cell membrane permeability, lysosomal mass/pH, and nuclear intensity (right column) changes. Colors range from dark green (values lower than 15% of maximum value measured) to bright green (30%), yellow (50%), bright orange (60%), dark orange (75%), and finally to red (values higher than 75% of maximum value). Heatmap values are normalized to the percentages of the positive control, and Z score is calculated as described in the Statistical Analysis section. Data represent three independent experiments performed in triplicate samples.

Doses are therefore expressed as 12×10^{-4}, 6×10^{-4}, and 1.2×10^{-4} μg/cell, respectively. No significant changes in cellular responses were detectable when 2D cell cultures were exposed to solutions containing equivalent amounts of DMSO, BSA, or Pluronic F68 for 72 h (Figure S3).

Cell Viability. Time-dependent effects of p- and o-SWNTs on the cell viability are shown in Figure 2. Both p- and o-SWNTs were demonstrated to influence considerably the cell viability, causing a significant decrease in cell count at all doses and for all nanotube dispersions after 24 and 72 h.

Cell Membrane Permeability. A significant increase in the cell membrane permeability was registered after a 72 h exposure to BSA-stabilized p-SWNT dispersions at all employed concentrations (Figure 2). These results indicate that the cytoplasmic membrane was compromised, while it remained unaffected after 24 h of exposure to DMSO- and Pluronic F68-stabilized dispersions of p-SWNTs at all examined time points. Significant changes were found in cells incubated with o-SWNTs, irrespective of the dispersing agent used (BSA, DMSO, or Pluronic F68) or the time point.

Lysosomal Mass/pH. No significant changes in the lysosomal mass/pH were seen in p- or o-SWNT-treated cultures (Figure 2).

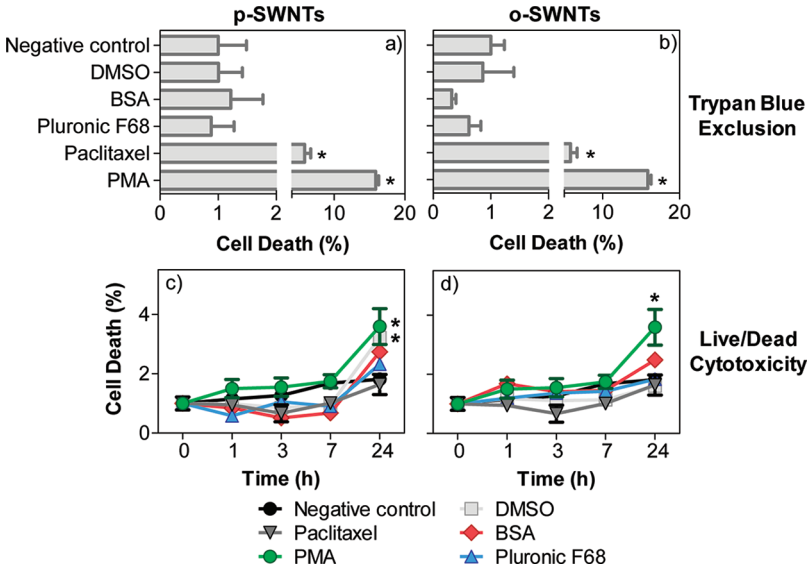

Figure 3. Cell death response quantified by (a, b) Trypan Blue exclusion and (c, d) live/dead cytotoxicity assays after exposure of 3D cell aggregates to (a, c) p- and (b, d) o-SWNTs at 1.2×10^{-4} μg/cell for 24 h *in situ* in the USWT. DMSO-, BSA-, and Pluronic F68-stabilized dispersions were tested.

Nuclear Intensity. As for the lysosomal mass/pH changes, marginal or nondetectable changes in the nuclear intensity were seen in all treatments with the exception of the 12×10^{-4} μg/cell dose, after 24 and 72 h exposure to p- and o-SWNTs, and of the 6×10^{-4} μg/cell dose in 2D cell cultures treated with DMSO-stabilized p-SWNT dispersions.

In summary, HCSA data consistently showed a considerable cytotoxic response after exposure to p- and o-SWNTs in a 2D cell culture of "macrophage-like" THP-1 cells. In particular, our HCSA data indicated that SWNTs can cause cell stress no matter the purity grade, the reactive groups present on the SWNT surface, the dispersing agent used, and/or the stability of the dispersion. Even though contradictory cytotoxicity results have been shown on the cellular response of macrophages in 2D cell models exposed to SWNTs,[69−72] our results were in agreement with some studies recently reported in the literature.[73,74] Additionally, although metal impurities seem to play a key role in the toxicity of SWNTs,[69,70,72,75] recent studies did identify the CNTs themselves as the principle cause of cytotoxicity in macrophages, rather than the catalysts.[74] Concentrations of p- and o-SWNTs tested in 2D cell cultures (120, 60, and 12 μg/mL, equivalent to 12×10^{-4}, 6×10^{-4}, and 1.2×10^{-4} μg/cell) were relatively high, but consistent with published studies. In recent *in vitro* studies on macrophage responses, SWNT concentrations varied from 0.3−10 μg/mL,[75] to 1−50 μg/mL,[74] 15−60 μg/mL,[70] 3 − 150 μg/mL,[76] 50−200 μg/mL,[77] and finally up to 0.12−0.5 mg/mL.[69] Also in the above referenced reports contradictory cytotoxicity responses have been detected (Table S11).

Cytotoxicity Assays of 3D Cell Culture Models *in Situ* in the Ultrasound Standing Wave Trap (USWT). *Trypan Blue Exclusion Assay*. 3D cell aggregates (nontreated, negative control) were 78% viable over 24 h in the USWT and remained as such following exposure to p- and o-SWNTs at 1.2×10^{-4} μg/cell (Figure 3a, b). Significant cell death was registered only when aggregates were treated with 1.7 μM paclitaxel (positive control) or phorbol-12-myristate-13-acetate (PMA, 0.5 mM). No differences in cell death levels were detected among the various stabilized SWNT suspensions under study.

Live/Dead Cytotoxity Assay. The live/dead cytotoxicity assay was performed in order to (1) validate the data obtained by the Trypan Blue exclusion assay, and (2) investigate whether the cell death was localized to the edges of the 3D aggregates, where cells were in direct contact with SWNTs. Quantification of cell death based on the epifluorescent images (Figure 3c, d) revealed no significant cytotoxic effects of the three differently stabilized p- and o-SWNT dispersions when compared to the negative control (cell death ranged between 20% and 44%). In parallel, the distribution of live and dead cells in SWNTs-treated 3D aggregates (Figure 4d) was similar to the negative control (Figure 4c) for all time points examined. Figure 4 shows representative results for a p-SWNT BSA-stabilized dispersion; consistent results were obtained for all the other SWNT samples.

Cytotoxicity Assays in 3D Cell Culture Models in Culture. In order to determine whether the different cellular responses observed in the 2D and 3D cellular models could be somehow associated with the different activation state of the THP-1 cells in the employed models (adherent "macrophage-like" cells in the 2D cell model and suspended monocytes in 3D cell aggregates), 3D cell aggregates of PMA-activated THP-1 cells were initially formed in the USWT, subsequently recovered from it, and exposed to p- and o-SWNTs in 24-well

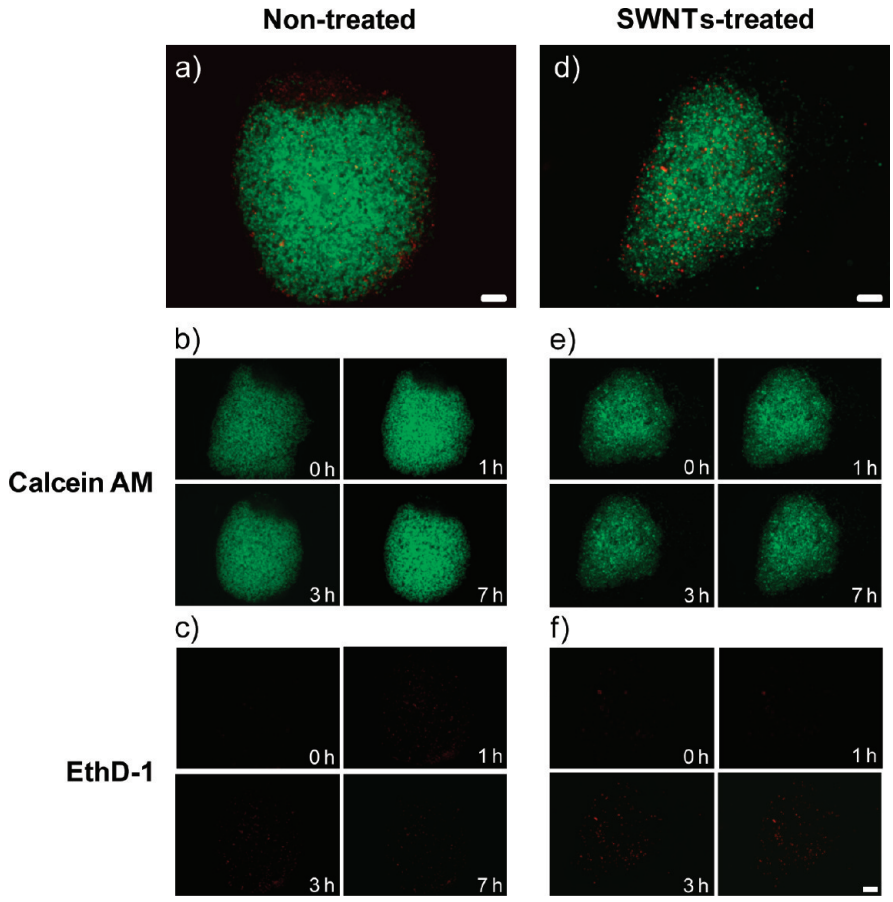

Figure 4. Representative epifluorescent images of (a–c) nontreated and (d, e) SWNT-treated 3D cell aggregates *in situ* in the USWT (a, d) after 24 h and (b, c, e, f) after 0, 1, 3, and 7 h, stained with Calcein AM (live cells) and EthD-1 (dead cells). SWNT concentration: 1.2×10^{-4} μg/cell; SWNT sample: p-SWNTs BSA-stabilized dispersion. Scale bars: 40 μm (10× magnification).

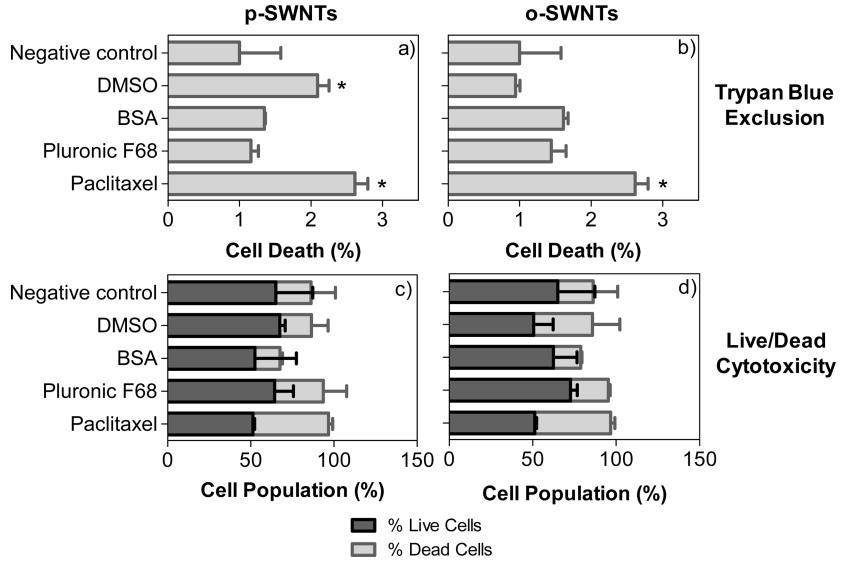

Figure 5. (a, b) Percentage (%) of cell death quantified by the Trypan Blue exclusion assay and (c, d) percent of live and dead cells detected by flow cytometry in 3D cell aggregates in culture exposed to DMSO-, BSA-, and Pluronic F68-stabilized dispersions of (a, c) p- and (b, d) o-SWNTs at 1.2×10^{-4} μg/cell for 24 h.

plates. Confocal microscopy analysis confirmed that PMA induced the activation of THP-1 cells within the 3D aggregates (Supporting Information).

Trypan Blue Exclusion Assay. Nontreated (negative control) 3D aggregates remained 80% viable over 24 h (similarly to the results obtained for 3D aggregates

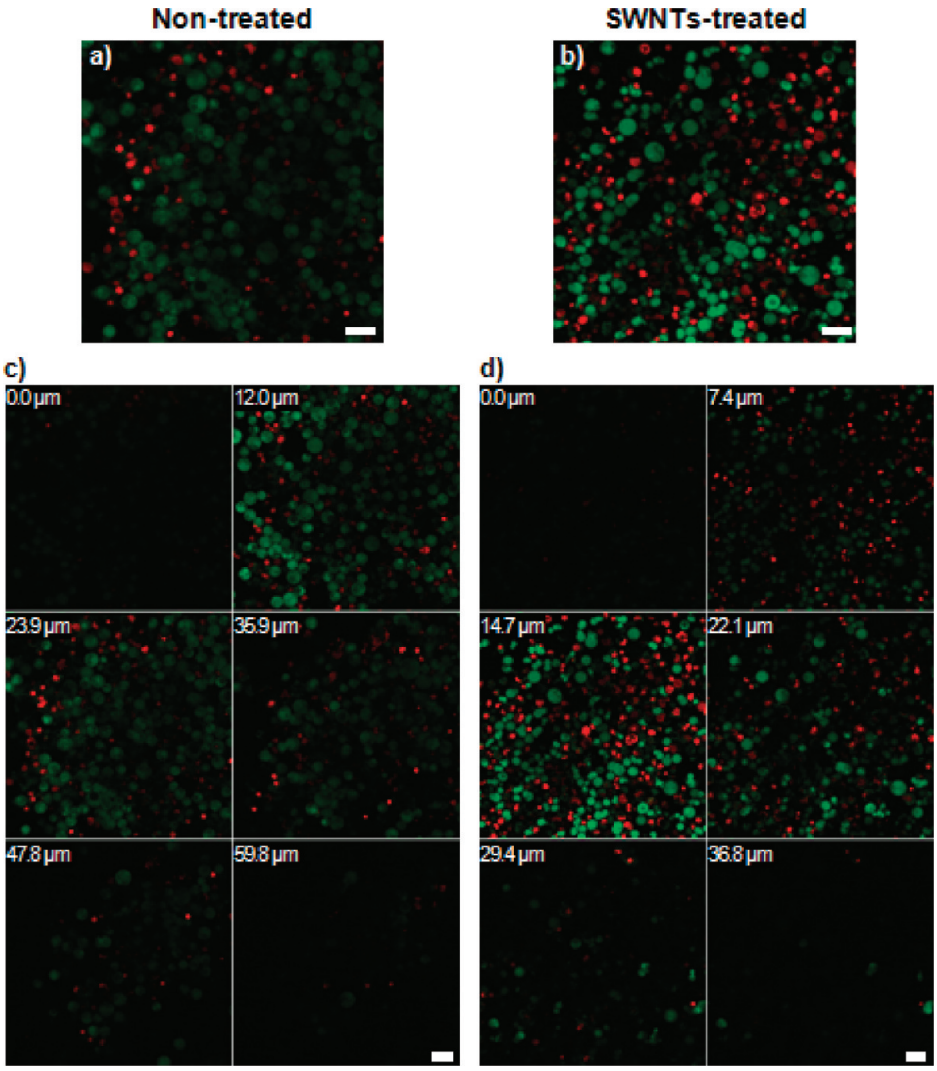

Figure 6. (a, b) Representative confocal images of (a) nontreated (negative control) and (b) SWNTs-treated 3D cell aggregates in culture after 24 h. (c, d) Gallery of stack images of (c) nontreated and (d) SWNTs-treated 3D cell aggregates. Micrographs in (c) and (d) are of the same 3D cell aggregate shown in (a) and (b), respectively. Live cells are seen in green; red indicates dead cells. Similar cell viability level can be seen in the two 3D cell aggregates. SWNTs sample: p-SWNTs BSA-stabilized dispersion. Scale bar: 20 μm (20$\times$ magnification).

in situ in the USWT). Exposure to p- and o-SWNTs did not significantly impair cell viability, with the exception of the DMSO-stabilized p-SWNT dispersion (Figure 5a, b).

Flow Cytometry of Live/Dead Cells. p-SWNTs and o-SWNTs did not cause any detectable cytotoxic outcome when compared to the nontreated aggregates (Figure 5c, d). The accompanying representative flow cytometric graphs are shown in the Supporting Information (Figure S1).

Live/dead staining analysis of 3D cell aggregates by confocal microscopy (Figure 6) further confirmed the flow cytometric data. Figure 6b and d are representative of all the SWNT dispersions tested in 3D cell aggregates in culture.

In summary, cell viability analysis (Figure 3 and Figure 5) consistently showed no detectable cytotoxic response or cell stress in 3D cell aggregates exposed to p- and o-SWNTs *in situ* in the USWTs or in culture. Furthermore, epifluorescent microscopy analysis provided evidence that cell death had a random distribution within SWNT-treated 3D aggregates *in situ* in the USWT (Figure 4) and in culture (Figure 6), and it was not localized to the areas where cells were in direct contact with the SWNTs.

Using the USWT we successfully fulfilled the necessity of reproducing one of the most important features of tissues *in vivo*, *i.e.*, its three-dimensional architecture, bridging the gap between *in vitro* cell models and complex *in vivo* studies[78] and offering added value to the *in vitro* prediction of SWNT toxicity. THP-1 cells spontaneously form aggregates of a few cells when cultured in suspension; these small spheroids can be recovered for experimentation. The use of 3D cell aggregates formed by the USWT satisfied, however, the necessity of developing a standardized protocol

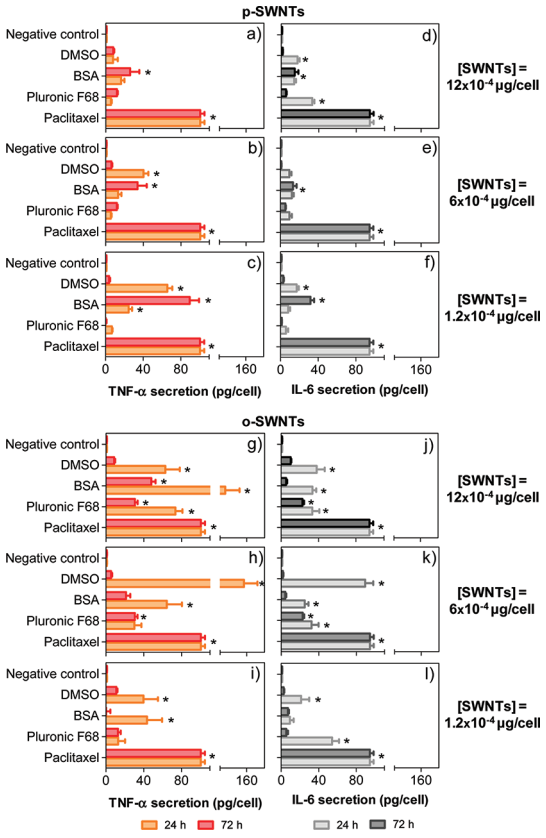

Figure 7. Release of (a–c, g–i) TNF-α and (d–f, j–l) IL-6 from 2D cell cultures after 24 and 72 h exposure to DMSO-, BSA-, and Pluronic F68-stabilized dispersions of (a–f) p- and (g–l) o-SWNTs at various concentrations: (a, d, g, j) 12 × 10^{-4}, (b, e, h, k) 6 × 10^{-4}, and (c, f, i, l) 1.2 × 10^{-4} µg/cell.

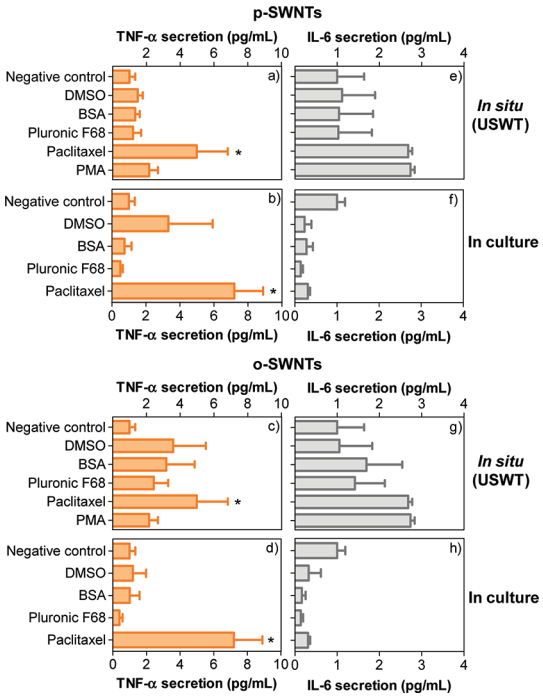

Figure 8. Release of (a–d) TNF-α and (d–h) IL-6 from 3D cell aggregates (a, c, e, g) *in situ* in the USWT or (b, d, f, h) in culture after 24 h exposure to DMSO-, BSA-, and Pluronic F68-stabilized dispersions of (a, b, e, f) p- and (c, d, g, h) o-SWNTs at 1.2 × 10^{-4} µg/cell.

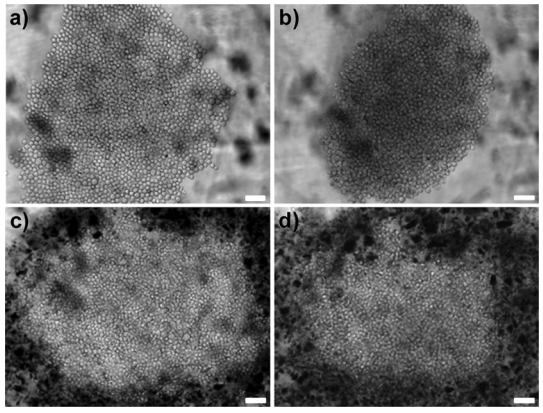

Figure 9. Typical 3D cell aggregates levitated in the USWT for (a) 5 min and (b) 24 h. After 24 h (b) the aggregate morphology was more closely packed. (c, d) SWNTs are visible as black agglomerates encapsulating the cell aggregate. Cell concentration: 10^6 cells/mL; SWNT concentration: 1.2 × 10^{-4} µg/cell. Scale bar: 40 µm (10× magnification).

that can be used to form well-defined and reproducible 3D aggregates of any cell type and/or of various cell types (cocultures). Since macrophages are not found as agglomerates in tissues, but dispersed with other cells, the USWT is the way toward the creation of 3D cell models of macrophages that are more representative of the human physiology. 3D cell aggregates formed by USWT give rise to a more "tissue-mimetic" cell model compared to conventional 3D cellular models. The USWT avoids in fact the introduction of polymeric 3D-cell-growth substrates[79–82] while allowing intercellular adhesive interactions to occur among cells.[83,84] Additionally, it permits monitoring the cytotoxic response of cells to SWNTs without any interference by sedimentation processes.[85] To this end, the different cytotoxic responses between the 2D and 3D cell models (both *in situ* in the USWT and in culture) presented here are most likely associated with the addition of the third dimension in the cell culture models and the extensive cell–cell interactions occurring in the 3D cell aggregates. It is a well-established fact that enhanced cell adhesion contacts commonly result in the increased population viability, in contrast to the loss of adhesion, or *anoikis*, leading to apoptosis.[86] In addition, some intrinsic limitations of *in vitro* models, including the methods of exposing cells, do not allow accurately reproducing the physiologically coordinated responses among various cell types in tissues and organs, and the delivery of SWNTs in one single dose does not reflect *in vivo* realistic conditions, where SWNTs are likely to accumulate gradually and at different concentrations due to different penetration thresholds through the different cellular layers. We acknowledge that the different toxicity thresholds between the 2D and 3D cell models could also be

associated with a decreased capability of penetration of p- and o-SWNTs within the 3D cell aggregates. Further studies are necessary, therefore, to clarify the cellular mechanisms involved in the response of 3D cell models to SWNTs.

Cytokine Expression. Indirect postexposure quantification of TNF-α and IL-6 expression levels by enzyme-linked immunosorbent assay (ELISA) allowed us to quantify the extent of inflammatory protein secretion related to the cell stress-induced signaling cascade and transduction activity. ELISA assays revealed a high secretion of pro-inflammatory cytokines (IL-6 and TNF-α) in 2D cell cultures following exposure to p- (Figure 7a–f) and o-SWNTs (Figure 7g–l) after 24 and 72 h exposure.

In contrast, no significant changes in IL-6 and TNF-α secretion were detected in 3D cell aggregates exposed to p- and o-SWNTs *in situ* in the USWT (Figure 8a, c, e, g) or in culture (Figure 8b, d, f, h) after 24 h exposure, which is in concert with the above-described data on comparative SWNT cytotoxicity in 2D and 3D models.

Control experiments were carried out to ensure that potential adsorption of proteins (such as cytokines) onto p-/o-SWNTs surface was not influencing the quantification of the concentrations of IL-6 and TNF-α secreted by THP-1 cells exposed to such nanomaterials (data shown in the Supporting Information).

CONCLUSIONS

Our study showed that p- and o-SWNTs were cytotoxic in 2D but not to the same extent in 3D cell culture models. As there is great uncertainty when conducting toxicological studies of CNTs (mainly due to the accuracy of the toxicity protocols and of the technologies employed until now), our study clearly demonstrated the importance of 3D cell culture models. The ability to rapidly and reproducibly form uniformly shaped and sized 3D aggregates by the USWT is undoubtedly of high interest and potential in the screening of the toxicity of SWNTs and other nanomaterials. In addition to the opportunities to more closely imitate realistic 3D tissue microenvironments, these 3D models can help in identifying and establishing necessary chemical modifications that are required to make such nanomaterials more biocompatible for a range of biological and medical applications.

MATERIALS AND METHODS

Chemicals and solvents were purchased from commercial sources (Sigma-Aldrich, Fisher Scientific, Invitrogen, and Calbiochem). As-produced HiPCO SWNTs (r-SWNTs) were purchased from Unidym (lot # R0546).

Purification and Oxidation of r-SWNTs. r-SWNTs were purified and oxidized following the procedure reported in previous studies[31,87] (Scheme 1).

p-SWNT and o-SWNT Dispersions. NIR-photoluminescence spectroscopy, zeta potential measurements, and toxicity tests were carried out on dispersions of p- and o-SWNTs in RPMI 1640 cell media (GIBCO, Bio Sciences Ltd., Ireland), with or without 100% bovine serum albumin (#A9647, Sigma-Aldrich) or 10% Pluronic F68 (SAFC Biosciences). Dry powder p-SWNTs and o-SWNTs were weighted and added to a 1:1 mixture of sterile DMSO and sterile DI water at a concentration of 2 mg/mL (stock solutions). Stock solutions were sonicated (sonic bath, 4 h) and aliquoted in three vials of 100 μL to prepare the working solutions as follows: (1) 5 μL of sterile BSA was added (BSA-stabilized dispersion); (2) 5 μL of Pluronic F68 was added (Pluronic F68-stabilized dispersion); (3) the stock solution was left unchanged (DMSO-stabilized dispersion). A 1.9 mL portion of RPMI 1640 cell media (supplemented with 2 mM L-glutamine, 10% fetal bovine serum (FBS), and 10 mg/mL penicillin–streptomycin) was mixed with solutions 1, 2, and 3, thus obtaining a final SWNT concentration of 120 μg/mL. Serial dilutions in supplemented RPMI 1640 cell media produced dispersions with concentration of 60 and 12 μg/mL of neutral pH. A schematic representation of the dispersion preparation is shown in Figure S2, together with the percentage composition of each solution obtained. Dispersions of p- and o-SWNTs in DI water for zeta potential measurements were prepared following the same protocol.

Physicochemical Characterizion. NIR-PL studies were carried out on p- and o-SWNTs dispersions in supplemented RPMI 1640 cell media ($[SWNTs]_i$ = 120 μg/mL) in a LOT ORIEL NS1 NanoSpectralyzer (Applied Nanofluorescence, USA) at an excitation wavelength (λ_{exc}) of 683 nm over a period of 1 h with an interval of 3.6 min. Measurements were also carried out at λ_{exc} values of 638 and 785 nm with similar results (data not shown). Zeta potential measurements were performed on p- and o-SWNTs solutions in DI water or in supplemented RPMI 1640 cell media by a Zetasizer Nanoseries Nano-ZS (Malvern Instruments, UK). Measurements were carried out in six replicates for each solution. Data are represented as average ± standard deviation.

Cell Culture. Human monocytic leukemia (THP-1) cells were obtained from the American Tissue Culture Collection (ATCC, USA). Briefly, THP-1 cells were cultured in suspension in modified RPMI 1640 media (supplemented with 2 mM L-glutamine, 10% FBS, and 10 mg/mL penicillin–streptomycin) and incubated at 37 °C and 5% CO_2. At 60% confluence, cells were diluted in modified RPMI 1640 media at concentrations appropriate for each experimental procedure. The passage number was restricted between 5 and 15.

2D Cell Culture Models. THP-1 cells were seeded in 96-well plates at a concentration of 20 000 cells/well (final volume: 200 μL/well) using a Matrix WellMate (ThermoFisher Scientific, USA) and activated with PMA 0.5 mM (Sigma-Aldrich) for 72 h to induce differentiation into adherent macrophages and stop their natural proliferation. After removing the cell media, adherent THP-1 cells were exposed to p- and o-SWNT dispersions. The final volume of solution added was 200 μL/well. Three different doses of p- and o-SWNTs were tested: 120, 60, and 12 μg/mL, corresponding to 12×10^{-4}, 6×10^{-4}, and 1.2×10^{-4} μg/cell, respectively. The anticancer agent paclitaxel (1.7 μM) (Sigma-Aldrich) was used as a positive control. Cells were exposed to SWNTs for 24 and 72 h.

Cytotoxicity Analysis of 2D Cell Cultures

- *Fluorescent staining of 2D cell cultures:* Supernatants were collected from each well for postexposure assays, and multiple washings with phosphate-buffered saline (PBS) were carried out in order to completely remove SWNTs from wells and avoid any potential interaction with the staining dyes. The multiparameter Cytotoxicity 1 HitKit HCSA reagent kit (ThermoFisher, USA) was used,[65,66] and staining was performed according to previously reported protocols.[9,66] This kit allows the detection of changes in many cellular properties.[9,66] Briefly, changes in cell viability are directly correlated to the toxic effects of the material tested. Following a toxic insult, cells may also respond with changes in nuclear intensity, and an increased nuclear intensity is generally associated with the cell nuclei collapse and cell stress.[88] Changes in the cell membrane permeability are often associated with an

ongoing toxic or apoptotic response, and the loss of cell membrane integrity is a common feature of marked cytotoxicity.[89] Finally, external agents can interfere with the normal cell physiology by affecting the mass, the number, or the function of organelles such as lysosomes.[90]

- *Imaging and HCSA analysis:* Measurements were carried out using the IN-Cell 1000 automated fluorescent microscope system (GE Healthcare, USA) and its associated analysis software (In Cell Analyzer System, GE Healthcare, USA). 96-well plates were read on IN-Cell Analyzer 1000 using three detection channels (461, 509, and 599 nm) with three different excitation filters (λ < 503 nm, λ > 509 nm, and λ > 599 nm). Ten random microscopic fields were sequentially acquired by the IN-Cell 1000 automated fluorescent microscope system at a magnification of 10×. Acquired images for each exposure time and dose were then analyzed by the IN-Cell Analyzer software according to previously reported procedures.[66,67]
- *Heatmaps:* Multiparameter HCSA data are presented as cluster heatmap graphical tables to highlight the potential differences in cellular responses among SWNT dispersions, concentrations, and exposure times.[91] For each SWNT solution the changes in cytotoxicity-associated parameters are presented in colorimetric gradients at the three different concentrations tested (Figure 2).

3D Cell Culture Model. A 1 mL amount of nonactivated THP-1 cells was transferred to an Eppendorf tube, centrifuged, and resuspended in supplemented, fresh RPMI 1640 cell media to a final concentration of 1×10^6 cells/mL.

- *Ultrasound standing wave trap and optical system:* USWT consisted of three features: a transducer (Ferroperm, Kvistgard, Denmark) in a housing of radial symmetry, an aqueous phase, and a reflector that provided optical access from the top as previously described.[79,92] The trap was driven with a function generator (Hewlett-Packard 33120A, UK). A fast, high-resolution XM10 camera (Soft Imaging System, SIS, GmbH, Munster, Germany) mounted on an Olympus BX51 M reflection epi-fluorescence microscope allowed observation in the direction of sound propagation (negative *z*-axis).[92] Images were captured by a standard PC equipped with the Cell-D image acquisition and processing software (Soft Imaging System, SIS, GmbH).
- *3D cell aggregates in situ in the USWT:* Cells were introduced into the USWT, the ultrasound was switched on for 10 min at 0.85 MPa (at which point the aggregate was mechanically robust[93]), and a 3D aggregate was formed (Figure 9a) as previously described.[79] In this work, aggregates consisted of approximately 36 000 THP-1 cells, while their size was *ca*. 1.5 mm in diameter. p- or o-SWNTs dispersions (DMSO-stabilized, BSA-stabilized, and Pluronic F68-stabilized suspensions) at a concentration of 120 μg/mL, corresponding to approximately 1.2×10^{-4} μg/cell, were introduced into the USWT and surrounded completely the 3D aggregate (Figure 9c). After 24 h, 3D THP-1 cell aggregates had a closely packed morphology with few small empty spaces (Figure 9b and d). 3D cell aggregates were exposed to SWNT samples for 24 h *in situ* in the USWT and monitored by microscopy. Aggregates perfused with fresh, supplemented RPMI 1640 cell media or paclitaxel served as negative and positive controls, respectively.
- *3D cell aggregates in culture:* In these series of experiments, THP-1 cells were treated with 2 μL of PMA (0.5 mM) to induce their differentiation into adherent macrophages. Following this, formation of 3D cell aggregates in the USWT proceeded as described above. However, aggregates were recovered from the trap after the 10 min period with a sterile 2 mL syringe (Plastipak, Becton Dickinson, UK), plated in 24-well plates (one 3D aggregate/well), and subsequently exposed to p- and o-SWNTs as described above. PMA-activated 3D aggregates had an average height of 25−30 μm.

Cytotoxicity Analysis of 3D Cell Cultures. All SWNT dispersions were tested on 3D aggregates in duplicate both *in situ* in the USWT and in culture.

- *Trypan Blue exclusion assay:* 3D aggregates were collected from the USWT and from the wells after exposure to p- or o-SWNTs, centrifuged, and resuspended in 10 μL of fresh RPMI 1640 cell media. A 10 μL amount of 0.4% Trypan Blue solution (Invitrogen, Molecular Probes, Oregon, USA) was then added. Blue-stained/dead cells and viable cells were counted, and percentage cell death was calculated as follows (eq 1):

$$\% \text{ cell death} = \frac{\text{dead cells}}{(\text{viable cells} + \text{dead cells})} \times 100 \quad (1)$$

  It is important to note that the Trypan Blue exclusion assay does not interact with SWNTs.[94]
- *Live/dead cytotoxity assay:* The live/dead cytotoxicity kit for mammalian cells (Invitrogen, Molecular Probes, Oregon, USA) was used. The kit is formed by two components: Calcein AM and ethidium homodimer-1 (EthD-1). SWNTs do not interact with the live/dead cytotoxicity assay.[94]
  For 3D cell aggregates *in situ* in the USWT, 2 μL of EthD-1 (2 mM) and 200 μL of Calcein AM (20 μM) were added to 800 μL of nonactivated THP-1 cells (10^6 cells/mL). After incubation at 37 °C/5% CO_2 for 30 min, 3D cell aggregate formation and perfusion of SWNTs proceeded as described above. 3D aggregates were examined at low magnification (5×) at 1, 3, 7, and 24 h. Quantification of live/death cells within each 3D cell aggregate was carried out using Image Pro7 software (Media Cybernetics Inc., USA) by applying advanced image filtering, object recognition, and counting algorithms on the collected fluorescent images.
  For 3D aggregates in culture, aggregates were collected from the wells, centrifuged, and resuspended in 800 μL of RPMI 1640 cell media. Then 2 μL of EthD-1 (2 mM) and 200 μL of Calcein AM (20 μM) were added. After incubation at 37 °C/5% CO_2 for 30 min, cells were washed by multiple steps of centrifugation and the percentages of live/dead cells was quantified by flow cytometry (Facs Canto II, BD, USA).
- *Confocal microscopy of 3D aggregates in culture:* 3D cell aggregates (PMA-activated) were formed in the USWT as described before, subsequently recovered and deposited in a 8-well glass-borosilicate chamber slide, and incubated for 24 h at 37 °C with or without p-/o-SWNTs. After 1 day in culture, 300 μL of staining solution (EthD-1 2 mM, Calcein AM 20 μM) was added to each well. After incubation in the dark for 45 min, aggregates were washed with sterile PBS. Specimens were immediately analyzed by a ZEISS 510 Meta confocal microscope (Carl Zeiss, Axiovert, Germany) equipped with a Zeiss LSM Image Browser. Two-channel qualitative confocal imaging was carried out by acquiring a series of Z-stack images.

Cytokine Secretion of 2D and 3D Cell Models. The concentrations of natural human interleukin-6 (IL-6) and human tumor necrosis factor-alpha (TNF-α) secreted by the exposed THP-1 cells were measured by ELISA assays (DuoSet ELISA development kit, R&D Systems: human TNF-α/TNFSF1A; human IL-6) and compared to the relevant controls. The assays were repeated in duplicate. The optical density of each well at 450 nm was determined by means of an Epoch microplate reader (Biotek, USA), calibrated against standards, and corrected by subtracting the optical aberration of the 96-well plastic plate. The cell count for 2D and 3D cell cultures was carried out by HCSA and Trypan Blue exclusion assay, respectively, in order to quantify the cytokine production as picograms per cell (pg/cell) or pictograms per mL (pg/mL) at the different concentrations and time points.

Statistical Analysis. A two-way analysis of variance (ANOVA) followed by a Bonferroni post-test analysis was carried out for all HCSA and cytokine assays (Prism; Graph-Pad Software Inc., USA). $p < 0.05$ was considered statistically significant and was denoted with (*) in the graphs. p values are reported in Tables S1−S10 (Supporting Information). HCSA and ELISA data, as well as the results obtained by Trypan Blue exclusion and live/dead assays, are presented as mean values ($n_{test} = 2$) ± standard error of the mean and normalized to the negative control. Due to the

large amount of information acquired by HCSA, a data mining and exploration platform was used (KNIME (http://KNIME.org, 2.0.3) in combination with a HiTS screening module (http://code.google.com/p/hits, 0.3.0) in order to screen and normalize all parameters under investigation as previously reported.[91] All measured parameters were normalized using the percentages of the positive control. Z score was used for scoring the normalized values. These scores were summarized using the mean function as follows: Z score = (x-mean)/SD, as previously reported.[95] Heatmaps (*i.e.*, graphical illustration in a colorimetric gradient table format) were adopted as the most suitable schematic representation to report on any statistical significance and variation from normalized controls based on their Z score value. Heatmap tables illustrate the range of variation of each quantified parameter from the minimum (green), through the mean (yellow), to the maximum (red) value.

Acknowledgment. This work was supported by Science Foundation Ireland under different schemes (PIYRA 07/Y12/I1052, CSET, and SRC), Higher Education Authority (HEA) under the PRTLI-4 program, the Health Research Board, and IRCSET (Postgraduate Research Scholarship to D.M.). Dr. Prina-Mello and Prof. Volkov acknowledge the financial support of the EU FP7 Project NAMDIATREAM (ref. 246469). We are grateful to Elisa Del Canto for the SWNTs. We also thank Dr. Anthony Davies and Dr. Bashir Mohammed (TCD-HCSA laboratory) for technical support and fruitful discussions.

Supporting Information Available: Tables of *p* values; summary of *in vitro* studies on macrophages exposed to SWNTs; schematic representation of the protocol employed for the preparation of SWNT dispersions; flow cytometry graphs; changes in cellular parameters in 2D cell cultures after exposure to surfactants; characterization of 3D cell aggregates in culture; control experiments for the ELISA assays. This material is available free of charge *via* the Internet at http://pubs.acs.org.

REFERENCES AND NOTES

1. Hirsch, A. The Era of Carbon Allotropes. *Nat. Mater.* **2010**, *9*, 868–871.
2. Walker, N. J.; Bucher, J. R. A 21st Century Paradigm for Evaluating the Health Hazards of Nanoscale Materials? *Toxicol Sci.* **2009**, *110*, 251–254.
3. Kipen, H. M.; Laskin, D. L. Smaller Is Not Always Better: Nanotechnology Yields Nanotoxicology. *Am. J. Physiol. Lung Cell. Mol. Physiol.* **2005**, *289*, L696–L697.
4. Hartung, T. Toxicology for the Twenty-First Century. *Nature* **2009**, *460*, 208–212.
5. Krug, H. F.; Wick, P. Nanotoxicology: An Interdisciplinary Challenge. *Angew. Chem., Int. Ed.* **2011**, *50*, 1260–1278.
6. Service, R. F. Nanotechnology—Can High-Speed Tests Sort out Which Nanomaterials Are Safe? *Science* **2008**, *321*, 1036–1037
7. Feliu, N.; Fadeel, B. Nanotoxicology: No Small Matter. *Nanoscale* **2010**, *2*, 2514–2520.
8. Shaw, S. Y.; Westly, E. C.; Pittet, M. J.; Subramanian, A.; Schreiber, S. L.; Weissleder, R. Perturbational Profiling of Nanomaterial Biologic Activity. *Proc. Natl. Acad. Sci. U. S. A.* **2008**, *105*, 7387–7392.
9. Jan, E.; Byrne, S. J.; Cuddihy, M.; Davies, A. M.; Volkov, Y.; Gun'ko, Y. K.; Kotov, N. A. High-Content Screening as a Universal Tool for Fingerprinting of Cytotoxicity of Nanoparticles. *ACS Nano* **2008**, *2*, 928–938.
10. George, S.; Pokhrel, S.; Xia, T.; Gilbert, B.; Ji, Z. X.; Schowalter, M.; Rosenauer, A.; Damoiseaux, R.; Bradley, K. A.; Madler, L.; *et al*. Use of a Rapid Cytotoxicity Screening Approach to Engineer a Safer Zinc Oxide Nanoparticle through Iron Doping. *ACS Nano* **2010**, *4*, 15–29.
11. Jones, C. F.; Grainger, D. W. *In Vitro* Assessments of Nanomaterial Toxicity. *Adv. Drug Delivery Rev.* **2009**, *61*, 438–456.
12. Zhang, T. T.; Stilwell, J. L.; Gerion, D.; Ding, L. H.; Elboudwarej, O.; Cooke, P. A.; Gray, J. W.; Alivisatos, A. P.; Chen, F. F. Cellular Effect of High Doses of Silica-Coated Quantum Dot Profiled with High Throughput Gene Expression Analysis and High Content Cellomics Measurements. *Nano Lett.* **2006**, *6*, 800–808.
13. Puzyn, T.; Rasulev, B.; Gajewicz, A.; Hu, X.; Dasari, T. P.; Michalkova, A.; Hwang, H.-M.; Toropov, A.; Leszczynska, D.; Leszczynski, J. Using Nano-Qsar to Predict the Cytotoxicity of Metal Oxide Nanoparticles. *Nat. Nanotechnol.* **2011**, DOI: 10.1038/nnano.2011.1010.
14. Pampaloni, F.; Reynaud, E. G.; Stelzer, E. H. K. The Third Dimension Bridges the Gap between Cell Culture and Live Tissue. *Nat. Rev. Mol. Cell Biol.* **2007**, *8*, 839–845.
15. Yamada, K. M.; Cukierman, E. Modeling Tissue Morphogenesis and Cancer in 3D. *Cell* **2007**, *130*, 601–610.
16. Beningo, K. A.; Dembo, M.; Wang, Y. L. Responses of Fibroblasts to Anchorage of Dorsal Extracellular Matrix Receptors. *Proc. Natl. Acad. Sci. U. S. A.* **2004**, *101*, 18024–18029.
17. Zhang, X. L.; Wang, W.; Yu, W. T.; Xie, Y. B.; Zhang, X. H.; Zhang, Y.; Ma, X. J. Development of an *in Vitro* Multicellular Tumor Spheroid Model Using Microencapsulation and Its Application in Anticancer Drug Screening and Testing. *Biotechnol. Prog.* **2005**, *21*, 1289–1296.
18. Muller, L.; Riediker, M.; Wick, P.; Mohr, M.; Gehr, P.; Rothen-Rutishauser, B. Oxidative Stress and Inflammation Response after Nanoparticle Exposure: Differences between Human Lung Cell Monocultures and an Advanced Three-Dimensional Model of the Human Epithelial Airways. *J. R. Soc. Interface* **2010**, *7*, S27–S40.
19. Blank, F.; Wehrli, M.; Lehmann, A.; Baum, O.; Gehr, P.; von Garnier, C.; Rothen-Rutishauser, B. M. Macrophages and Dendritic Cells Express Tight Junction Proteins and Exchange Particles in an *in Vitro* Model of the Human Airway Wall. *Immunobiology* **2011**, *216*, 86–95.
20. Lee, J.; Lilly, G. D.; Doty, R. C.; Podsiadlo, P.; Kotov, N. A. *In Vitro* Toxicity Testing of Nanoparticles in 3D Cell Culture. *Small* **2009**, *5*, 1213–1221.
21. Sanchez, V. C.; Weston, P.; Yan, A. H.; Hurt, R. H.; Kane, A. B. A 3-Dimensional *in Vitro* Model of Epithelioid Granulomas Induced by High Aspect Ratio Nanomaterials. *Part. Fibre Toxicol.* **2011**, *8*.
22. Zuin, S.; Micheletti, C.; Critto, A.; Pojana, G.; Johnston, H.; Stone, V.; Tran, L.; Marcomini, A. Weight of Evidence Approach for the Relative Hazard Ranking of Nanomaterials. *Nanotoxicology* **2011**, *5*, 445–458.
23. Plowden, J.; Renshaw-Hoelscher, M.; Engleman, C.; Katz, J.; Sambhara, S. Innate Immunity in Aging: Impact on Macrophage Function. *Aging Cell* **2004**, *3*, 161–167.
24. Oberdorster, G.; Sharp, Z.; Atudorei, V.; Elder, A.; Gelein, R.; Lunts, A.; Kreyling, W.; Cox, C. Extrapulmonary Translocation of Ultrafine Carbon Particles Following Whole-Body Inhalation Exposure of Rats. *J. Toxicol. Environ. Health A* **2002**, *65*, 1531–1543.
25. Stone, V.; Johnston, H.; Schins, R. P. F. Development of *in Vitro* Systems for Nanotoxicology: Methodological Considerations. *Crit. Rev. Toxicol.* **2009**, *39*, 613–626.
26. Kagan, V. E.; Bayir, H.; Shvedova, A. A. Nanomedicine and Nanotoxicology: Two Sides of the Same Coin. *Nanomedicine* **2005**, *1*, 313–316.
27. Tian, F.; Cui, D.; Schwarz, H.; Estrada, G. G.; Kobayashi, H. Cytotoxicity of Single-Wall Carbon Nanotubes on Human Fibroblasts. *Toxicol. in Vitro* **2006**, *20*, 1202–1212.
28. Cui, H.-F.; Vashist, S. K.; Al-Rubeaan, K.; Luong, J. H. T.; Sheu, F.-S. Interfacing Carbon Nanotubes with Living Mammalian Cells and Cytotoxicity Issues. *Chem. Res. Toxicol.* **2010**, *23*, 1131–1147.
29. Koyama, S.; Kim, Y. A.; Hayashi, T.; Takeuchi, K.; Fujii, C.; Kuroiwa, N.; Koyama, H.; Tsukahara, T.; Endo, M. *In Vivo* Immunological Toxicity in Mice of Carbon Nanotubes with Impurities. *Carbon* **2009**, *47*, 1365–1372.
30. Kolosnjaj-Tabi, J.; Hartman, K. B.; Boudjemaa, S.; Ananta, J. S.; Morgant, G.; Szwarc, H.; Wilson, L. J.; Moussa, F. *In Vivo* Behavior of Large Doses of Ultrashort and Full-Length Single-Walled Carbon Nanotubes after Oral and Intraperitoneal Administration to Swiss Mice. *ACS Nano* **2010**, *4*, 1481–1492.
31. Movia, D.; Del Canto, E.; Giordani, S. Purified and Oxidized Single-Walled Carbon Nanotubes as Robust Near-IR

Fluorescent Probes for Molecular Imaging. *J. Phys. Chem. C* **2010**, *114*, 18407–18413.
32. Oberdorster, G.; Maynard, A.; Donaldson, K.; Castranova, V.; Fitzpatrick, J.; Ausman, K.; Carter, J.; Karn, B.; Kreyling, W.; Lai, D.; *et al.* Principles for Characterizing the Potential Human Health Effects from Exposure to Nanomaterials: Elements of a Screening Strategy. *Part. Fibre Toxicol.* **2005**, *2*, 8.
33. Rivera Gil, P.; Oberdorster, G.; Elder, A.; Puntes, V.; Parak, W. J. Correlating Physico-Chemical with Toxicological Properties of Nanoparticles: The Present and the Future. *ACS Nano* **2010**, *4*, 5527–5531.
34. Nel, A. E.; Madler, L.; Velegol, D.; Xia, T.; Hoek, E. M.; Somasundaran, P.; Klaessig, F.; Castranova, V.; Thompson, M. Understanding Biophysicochemical Interactions at the Nano-Bio Interface. *Nat. Mater.* **2009**, *8*, 543–557.
35. Hurt, R. H.; Monthioux, M.; Kane, A. Toxicology of Carbon Nanomaterials: Status, Trends, and Perspectives on the Special Issue. *Carbon* **2006**, *44*, 1028–1033.
36. Hankin, S. M.; Boraschi, D.; Duschl, A.; Lehr, C. M.; Lichtenbeld, H., Towards Nanotechnology Regulation—Publish the Unpublishable. *Nano Today* **2011**, DOI: 10.1016/j.nantod.2011.1003.1002.
37. Alpatova, A. L.; Shan, W. Q.; Babica, P.; Upham, B. L.; Rogensues, A. R.; Masten, S. J.; Drown, E.; Mohanty, A. K.; Alocilja, E. C.; Tarabara, V. V. Single-Walled Carbon Nanotubes Dispersed in Aqueous Media *Via* Non-Covalent Functionalization: Effect of Dispersant on the Stability, Cytotoxicity, and Epigenetic Toxicity of Nanotube Suspensions. *Water Res.* **2010**, *44*, 505–520.
38. Mutlu, G. M.; Budinger, G. R. S.; Green, A. A.; Urich, D.; Soberanes, S.; Chiarella, S. E.; Alheid, G. F.; McCrimmon, D. R.; Szleifer, I.; Hersam, M. C. Biocompatible Nanoscale Dispersion of Single-Walled Carbon Nanotubes Minimizes *in Vivo* Pulmonary Toxicity. *Nano Lett.* **2010**, *10*, 1664–1670.
39. Singh, P.; Campidelli, S.; Giordani, S.; Bonifazi, D.; Bianco, A.; Prato, M. Organic Functionalisation and Characterisation of Single-Walled Carbon Nanotubes. *Chem. Soc. Rev.* **2009**, *38*, 2214–2230.
40. Britz, D. A.; Khlobystov, A. N. Noncovalent Interactions of Molecules with Single Walled Carbon Nanotubes. *Chem. Soc. Rev.* **2006**, *35*, 637–659.
41. Herzog, E.; Byrne, H. J.; Davoren, M.; Casey, A.; Duschl, A.; Oostingh, G. J. Dispersion Medium Modulates Oxidative Stress Response of Human Lung Epithelial Cells Upon Exposure to Carbon Nanomaterial Samples. *Toxicol. Appl. Pharmacol.* **2009**, *236*, 276–281.
42. Dong, L. F.; Witkowski, C. M.; Craig, M. M.; Greenwade, M. M.; Joseph, K. L. Cytotoxicity Effects of Different Surfactant Molecules Conjugated to Carbon Nanotubes on Human Astrocytoma Cells. *Nanoscale Res. Lett.* **2009**, *4*, 1517–1523.
43. Valenti, L. E.; Fiorito, P. A.; Garcia, C. D.; Giacomelli, C. E. The Adsorption-Desorption Process of Bovine Serum Albumin on Carbon Nanotubes. *J. Colloid Interface Sci.* **2007**, *307*, 349–356.
44. Zhao, X. C.; Liu, R. T.; Chi, Z. X.; Teng, Y.; Qin, P. F. New Insights into the Behavior of Bovine Serum Albumin Adsorbed onto Carbon Nanotubes: Comprehensive Spectroscopic Studies. *J. Phys. Chem. B* **2010**, *114*, 5625–5631.
45. Matsuura, K.; Saito, T.; Okazaki, T.; Ohshima, S.; Yumura, M.; Iijima, S. Selectivity of Water-Soluble Proteins in Single-Walled Carbon Nanotube Dispersions. *Chem. Phys. Lett.* **2006**, *429*, 497–502.
46. Wang, X.; Xia, T.; Ntim, S. A.; Ji, Z.; George, S.; Meng, H.; Zhang, H.; Castranova, V.; Mitra, S.; Nel, A. E. Quantitative Techniques for Assessing and Controlling the Dispersion and Biological Effects of Multiwalled Carbon Nanotubes in Mammalian Tissue Culture Cells. *ACS Nano* **2010**, *4*, 7241–7252.
47. Carter, D. C.; Ho, J. X. Structure of Serum-Albumin. *Adv. Protein Chem.* **1994**, *45*, 153–203.
48. Peter, T. In *All About Albumin: Biochemistry, Genetics, and Medical Applications*; Academic Press: San Diego, 1996; p 432.
49. Edri, E.; Regev, O. pH Effects on BSA-Dispersed Carbon Nanotubes Studied by Spectroscopy-Enhanced Composition Evaluation Techniques. *Anal. Chem.* **2008**, *80*, 4049–4054.
50. Parnaud, G.; Tache, S.; Peiffer, G.; Corpet, D. E. Pluronic F68 Block Polymer, a Very Potent Suppressor of Carcinogenesis in the Colon of Rats and Mice. *Br. J. Cancer* **2001**, *84*, 90–93.
51. Anson-Casaos, A.; Gonzalez-Dominguez, J. M.; Martinez, M. T. Separation of Single-Walled Carbon Nanotubes from Graphite by Centrifugation in a Surfactant or in Polymer Solutions. *Carbon* **2010**, *48*, 2917–2924.
52. Moore, V. C.; Strano, M. S.; Haroz, E. H.; Hauge, R. H.; Smalley, R. E.; Schmidt, J.; Talmon, Y. Individually Suspended Single-Walled Carbon Nanotubes in Various Surfactants. *Nano Lett.* **2003**, *3*, 1379–1382.
53. Bardi, G.; Tognini, P.; Ciofani, G.; Raffa, V.; Costa, M.; Pizzorusso, T. Pluronic-Coated Carbon Nanotubes Do Not Induce Degeneration of Cortical Neurons *in Vivo* and *in Vitro*. *Nanomedicine* **2009**, *5*, 96–104.
54. O'Connell, M. J.; Bachilo, S. M.; Huffman, C. B.; Moore, V. C.; Strano, M. S.; Haroz, E. H.; Rialon, K. L.; Boul, P. J.; Noon, W. H.; Kittrell, C.; *et al.* Band Gap Fluorescence from Individual Single-Walled Carbon Nanotubes. *Science* **2002**, *297*, 593–596.
55. Hasan, T.; Scardaci, V.; Tan, P. H.; Rozhin, A. G.; Milne, W. I.; Ferrari, A. C. Stabilization and "Debundling" of Single-Wall Carbon Nanotube Dispersions in N-Methyl-2-Pyrrolidone (NMP) by Polyvinylpyrrolidone (PVP). *J. Phys. Chem. C* **2007**, *111*, 12594–12602.
56. Weisman, R. B.; Bachilo, S. M.; Tsyboulski, D. Fluorescence Spectroscopy of Single-Walled Carbon Nanotubes in Aqueous Suspension. *Appl. Phys. A: Mater. Sci. Process* **2004**, *78*, 1111–1116.
57. Tan, P. H.; Rozhin, A. G.; Hasan, T.; Hu, P.; Scardaci, V.; Milne, W. I.; Ferrari, A. C., Photoluminescence Spectroscopy of Carbon Nanotube Bundles: Evidence for Exciton Energy Transfer. *Phys. Rev. Lett.* **2007**, *99*.
58. Paredes, J. I.; Burghard, M. Dispersions of Individual Single-Walled Carbon Nanotubes of High Length. *Langmuir* **2004**, *20*, 5149–5152.
59. Saleh, N. B.; Pfefferle, L. D.; Elimelech, M. Influence of Biomacromolecules and Humic Acid on the Aggregation Kinetics of Single-Walled Carbon Nanotubes. *Environ. Sci. Technol.* **2010**, *44*, 2412–2418.
60. Sano, M.; Okamura, J.; Shinkai, S. Colloidal Nature of Single-Walled Carbon Nanotubes in Electrolyte Solution: The Schulze-Hardy Rule. *Langmuir* **2001**, *17*, 7172–7173.
61. Hu, H.; Yu, A. P.; Kim, E.; Zhao, B.; Itkis, M. E.; Bekyarova, E.; Haddon, R. C. Influence of the Zeta Potential on the Dispersability and Purification of Single-Walled Carbon Nanotubes. *J. Phys. Chem. B* **2005**, *109*, 11520–11524.
62. Mamedov, A. A.; Kotov, N. A.; Prato, M.; Guldi, D. M.; Wicksted, J. P.; Hirsch, A. Molecular Design of Strong Single-Wall Carbon Nanotube/Polyelectrolyte Multilayer Composites. *Nat. Mater.* **2002**, *1*, 190–194.
63. Smith, B.; Wepasnick, K.; Schrote, K. E.; Bertele, A. H.; Ball, W. P.; O'Melia, C.; Fairbrother, D. H. Colloidal Properties of Aqueous Suspensions of Acid-Treated, Multi-Walled Carbon Nanotubes. *Environ. Sci. Technol.* **2009**, *43*, 819–825.
64. *Methods of Test for Zeta Potential of Colloids in Water and Waste Water*; American Society for Testing and Materials, **1985**; Vol. ASTM D4187-82.
65. Abraham, V. C.; Taylor, D. L.; Haskins, J. R. High Content Screening Applied to Large-Scale Cell Biology. *Trends Biotechnol.* **2004**, *22*, 15–22.
66. Movia, D.; Prina-Mello, A.; Volkov, Y.; Giordani, S. Determination of Spiropyran Cytotoxicity by High Content Screening and Analysis for Safe Application in Bionanosensing. *Chem. Res. Toxicol.* **2010**, *23*, 1459–1466.
67. Byrne, F.; Prina-Mello, A.; Whelan, A.; Mohamed, B. M.; Davies, A.; Gun'ko, Y. K.; Coey, J. M. D.; Volkov, Y. High Content Analysis of the Biocompatibility of Nickel Nanowires. *J. Magn. Magn. Mater.* **2009**, *321*, 1341–1345.

68. Williams, Y.; Sukhanova, A.; Nowostawska, M.; Davies, A. M.; Mitchell, S.; Oleinikov, V.; Gun'ko, Y.; Nabiev, I.; Kelleher, D.; Volkov, Y. Probing Cell-Type-Specific Intracellular Nanoscale Barriers Using Size-Tuned Quantum Dots. *Small* **2009**, *5*, 2581–2588.
69. Kagan, V. E.; Tyurina, Y. Y.; Tyurin, V. A.; Konduru, N. V.; Potapovich, A. I.; Osipov, A. N.; Kisin, E. R.; Schwegler-Berry, D.; Mercer, R.; Castranova, V.; *et al*. Direct and Indirect Effects of Single Walled Carbon Nanotubes on Raw 264.7 Macrophages: Role of Iron. *Toxicol. Lett.* **2006**, *165*, 88–100.
70. Fiorito, S.; Serafino, A.; Andreola, F.; Bernier, P. Effects of Fullerenes and Single-Wall Carbon Nanotubes on Murine and Human Macrophages. *Carbon* **2006**, *44*, 1100–1105.
71. Dutta, D.; Sundaram, S. K.; Teeguarden, J. G.; Riley, B. J.; Fifield, L. S.; Jacobs, J. M.; Addleman, S. R.; Kaysen, G. A.; Moudgil, B. M.; Weber, T. J. Adsorbed Proteins Influence the Biological Activity and Molecular Targeting of Nanomaterials. *Toxicol. Sci.* **2007**, *100*, 303–315.
72. Pulskamp, K.; Diabate, S.; Krug, H. F. Carbon Nanotubes Show No Sign of Acute Toxicity but Induce Intracellular Reactive Oxygen Species in Dependence on Contaminants. *Toxicol. Lett.* **2007**, *168*, 58–74.
73. Jia, G.; Wang, H. F.; Yan, L.; Wang, X.; Pei, R. J.; Yan, T.; Zhao, Y. L.; Guo, X. B. Cytotoxicity of Carbon Nanomaterials: Single-Wall Nanotube, Multi-Wall Nanotube, and Fullerene. *Environ. Sci. Technol.* **2005**, *39*, 1378–1383.
74. Dong, P. X.; Wan, B.; Guo, L. H. *In vitro* Toxicity of Acid-Functionalized Single-Walled Carbon Nanotubes: Effects on Murine Macrophages and Gene Expression Profiling. *Nanotoxicology* **2011**, DOI:10.3109/17435390.2011.573101.
75. Porter, A. E.; Gass, M.; Bendall, J. S.; Muller, K.; Goode, A.; Skepper, J. N.; Midgley, P. A.; Welland, M. Uptake of Noncytotoxic Acid-Treated Single-Walled Carbon Nanotubes into the Cytoplasm of Human Macrophage Cells. *ACS Nano* **2009**, *3*, 1485–1492.
76. Wang, G.; Dewilde, A. H.; Zhang, J. P.; Pal, A.; Vashist, M.; Bello, D.; Marx, K. A.; Braunhut, S. J.; Therrien, J. M., A Living Cell Quartz Crystal Microbalance Biosensor for Continuous Monitoring of Cytotoxic Responses of Macrophages to Single-Walled Carbon Nanotubes. *Part. Fibre Toxicol.* **2011**, *8*.
77. Hamilton, R. F.; Buford, M. C.; Wood, M. B.; Arnone, B.; Morandi, M.; Holian, A. Engineered Carbon Nanoparticles Alter Macrophage Immune Function and Initiate Airway Hyper-Responsiveness in the Balb/C Mouse Model. *Nanotoxicology* **2007**, *1*, 104–117.
78. Murphy, F. A.; Poland, C. A.; Duffin, R.; Al-Jamal, K. T.; Ali-Boucetta, H.; Nunes, A.; Byrne, F.; Prina-Mello, A.; Volkov, Y.; Li, S.; *et al*. Length-Dependent Retention of Carbon Nanotubes in the Pleural Space of Mice Initiates Sustained Inflammation and Progressive Fibrosis on the Parietal Pleura. *Am. J. Pathol.* **2011**, *178*, 2587–2600.
79. Bazou, D.; Foster, G. A.; Ralphs, J. R.; Coakley, W. T. Molecular Adhesion Development in a Neural Cell Monolayer Forming in an Ultrasound Trap. *Mol. Membr. Biol.* **2005**, *22*, 229–240.
80. Bazou, D.; Dowthwaite, G. P.; Khan, I. M.; Archer, C. W.; Ralphs, J. R.; Coakley, W. T. Gap Junctional Intercellular Communication and Cytoskeletal Organization in Chondrocytes in Suspension in an Ultrasound Trap. *Mol. Membr. Biol.* **2006**, *23*, 195–205.
81. Coakley, W. T.; Bazou, D.; Morgan, J.; Foster, G. A.; Archer, C. W.; Powell, K.; Borthwick, K. A. J.; Twomey, C.; Bishop, J. Cell-Cell Contact and Membrane Spreading in an Ultrasound Trap. *Colloids Surf., B* **2004**, *34*, 221–230.
82. Liu, R.; Kwok, Y. L.; Li, Y.; Lao, T. T.; Zhang, X.; Dai, X. Q. A Three-Dimensional Biomechanical Model for Numerical Simulation of Dynamic Pressure Functional Performances of Graduated Compression Stocking (GCS). *Fibers Polym.* **2006**, *7*, 389–397.
83. Edwards, G. O.; Bazou, D.; Kuznetsova, L. A.; Coakley, W. T. Cell Adhesion Dynamics and Actin Cytoskeleton Reorganization in Hepg2 Cell Aggregates. *Cell Commun. Adhes.* **2007**, *14*, 9–20.
84. Kuznetsova, L. A.; Bazou, D.; Edwards, G. O.; Coakley, W. T. Multiple Three-Dimensional Mammalian Cell Aggregates Formed Away from Solid Substrata in Ultrasound Standing Waves. *Biotechnol. Prog.* **2009**, *25*, 834–841.
85. Cho, E. C.; Zhang, Q.; Xia, Y. The Effect of Sedimentation and Diffusion on Cellular Uptake of Gold Nanoparticles. *Nat. Nanotechnol.* **2011**.
86. Liotta, L. A.; Kohn, E. Anoikis: Cancer and the Homeless Cell. *Nature* **2004**, *430*, 973–974.
87. Movia, D.; Del Canto, E.; Giordani, S. Spectroscopy of Single-Walled Carbon Nanotubes in Aqueous Surfactant Dispersion. *Phys. Status Solidi B* **2009**, *246*, 2704–2707.
88. Majno, G.; Joris, I. Apoptosis, Oncosis, and Necrosis—an Overview of Cell-Death. *Am. J. Pathol.* **1995**, *146*, 3–15.
89. Mingeotleclercq, M. P.; Brasseur, R.; Schanck, A. Molecular-Parameters Involved in Aminoglycoside Nephrotoxicity. *J. Toxicol. Environ. Health* **1995**, *44*, 263–300.
90. Reasor, M. J. A Review of the Biology and Toxicologic Implications of the Induction of Lysosomal Lamellar Bodies by Drugs. *Toxicol. Appl. Pharmacol.* **1989**, *97*, 47–56.
91. Mohamed, B. M.; Verma, N. K.; Prina-Mello, A.; Williams, Y.; Davies, A. M.; Bakos, G.; Tormey, L.; Edwards, C.; Hanrahan, J.; Salvati, A.; *et al*. Activation of Stress-Related Signalling Pathway in Human Cells Upon SiO_2 Nanoparticles Exposure as an Early Indicator of Cytotoxicity. *J. Nanobiotechnol.* **2011**, *9*, 29–43.
92. Bazou, D.; Kuznetsova, L. A.; Coakley, W. T. Physical Enviroment of 2-D Animal Cell Aggregates Formed in a Short Pathlength Ultrasound Standing Wave Trap. *Ultrasound Med. Biol.* **2005**, *31*, 423–430.
93. Bazou, D.; Santos-Martinez, M. J.; Medina, C.; Radomski, M. W. Elucidation of Flow-Mediated Tumour Cell-Induced Platelet Aggregation Using an Ultrasound Standing Wave Trap. *Br. J. Pharmacol.* **2011**, *162*, 1577–1589.
94. Monteiro-Riviere, N. A.; Inman, A. O.; Zhang, L. W. Limitations and Relative Utility of Screening Assays to Assess Engineered Nanoparticle Toxicity in a Human Cell Line. *Toxicol. Appl. Pharmacol.* **2009**, *234*, 222–235.
95. Birmingham, A.; Selfors, L. M.; Forster, T.; Wrobel, D.; Kennedy, C. J.; Shanks, E.; Santoyo-Lopez, J.; Dunican, D. J.; Long, A.; Kelleher, D.; *et al*. Statistical Methods for Analysis of High-Throughput RNA Interference Screens. *Nat. Methods* **2009**, *6*, 569–575.